Multi-User Long-Distance sub-THz Wireless Communication

J. Dittmer[1], A. Bhutani[2], F. Beuthan[1], L. Valenziano[2],
S. Wagner[3], A. Tessmann[3], C. Koos[1], T. Zwick[2], S. Randel[1]

[1]Institute of Photonics and Quantum Electronics (IPQ), Karlsruhe Institute of Technology (KIT), Germany
[2]Institute of Radio Frequency Engineering and Electronics (IHE), Karlsruhe Institute of Technology (KIT), Germany
[3]Fraunhofer Institute for Applied Solid State Physics IAF, Freiburg, Germany

***Abstract*—In this paper we present the first point-to-multipoint sub-THz wireless communication link capable of simultaneously transmitting data to multiple users over several meters at tens of gigabits per second. The sub-THz wireless link employs an optoelectronic transmitter that generates digital subcarriers by modulating a single free-running laser with a high-bandwidth electro-optic IQ modulator. A uni-traveling-carrier photodiode downconverts the transmitted signal from the optical to the sub-THz domain, and the signal is transmitted by a lens-integrated leaky-wave antenna, offering a gain of up to 30 dBi and a wide beam-steering range of approximately 51 degrees in the horizontal plane. The optoelectronic transmitter can simultaneously address multiple receiver units, i.e., users, hence enabling efficient multi-user operation. A sub-THz electronic receiver unit operating from 280 to 320 GHz is used for reception. In a proof-of-concept experiment, the sub-THz wireless link is implemented in a lecture hall scenario with one transmitter and two receiver units. The distance between the transmitter and receivers is 16 m, with the two receivers having a maximum spacing of 3.3 m. Measurements have been conducted for single-, dual-, and up to four-user configurations using QPSK and 16-QAM modulation schemes. To the best of the authors' knowledge, record-high data rates of up to 80 Gbps for a single-user, 40 Gbps for dual-users, and 20 Gbps for four users are demonstrated for the first time in a sub-THz point-to-multipoint system.**

***Index Terms*—Terahertz communications, photonics, microwave photonics, 6G mobile communication, point-to-multipoint, communication, wireless communication, multi-user, frequency beam-steering.**

I. Introduction

In a hyper-connected society powered by 6G mobile networks, high speed wireless communication is essential for various applications such as indoor access and outdoor small cell networks [1]–[3], supporting, for e.g., high-bandwidth augmented and virtual reality content. To meet this need, high-speed sub-THz wireless links are a particularly attractive option, especially in the context of mobile fronthaul networks and especially in indoor access networks for multi-user applications. Specifically, high data rates of tens of gigabits per second require large absolute bandwidths, which are available in the sub-THz range between $100\,\mathrm{GHz}$ and $1\,\mathrm{THz}$. In particular, the frequency range of $200\,\mathrm{GHz}$ to $325\,\mathrm{GHz}$ is especially attractive for high-speed wireless links due to low atmospheric attenuation, of less than $5\,\mathrm{dB/km}$ under typical weather conditions compared to higher frequencies in the sub-THz range, where water absorption becomes more and more problematic. As the frequency increases, the beam divergence decreases, resulting in a pencil beam antenna pattern, which improves directivity and reduces mutual interference, thus preventing cross talk. Furthermore, a variety of sub-THz sources, including solid-state electronic and optoelectronic devices have become available over the past two decades, which makes the sub-THz range attractive for future wireless applications [4], [5]. Additionally, the first IEEE standard for wireless communications in the sub-THz frequency range, IEEE Std. 802.15.3d, has been recently defined specifically for the frequency range of $253\,\mathrm{GHz}$ to $322\,\mathrm{GHz}$ [2].

State-of-the-art high-speed experiments in the sub-THz range using solid-state electronic devices based on III-V semiconductors (i.e. InGaAs mHEMT technology) show data rates of $64\,\mathrm{Gbps}$ over a $850\,\mathrm{m}$ point-to-point (P2P) link and $96\,\mathrm{Gbps}$ over a $40\,\mathrm{m}$ P2P link at a carrier frequency of $240\,\mathrm{GHz}$ [6]. Furthermore, a $120\,\mathrm{Gbps}$ $9.8\,\mathrm{m}$ link using the same technology has been demonstrated at $296\,\mathrm{GHz}$ [7]. Recently, a $52\,\mathrm{m}$ long sub-THz P2P link with a bandwidth of $66\,\mathrm{GHz}$ and a center frequency of $300\,\mathrm{GHz}$ has been demonstrated achieving a record high data rate of $200\,\mathrm{Gbps}$ using high-bandwidth optoelectronic components for sub-THz signal generation at the transmitter and a receiver based on solid-state electronics [8]. Notably, the vast majority of these works in the sub-THz range demonstrate high-capacity, long-distance P2P links with a single transmitter and a single user [6]–[8].

Unlike P2P links, which typically use high-gain antennas at a stationary transmitter and a fixed receiver, point-to-multipoint (P2MP) links for multi-user scenarios require steering of the antenna beam over a given angular range. Conventional beam steering is achieved using mechanical scanning technology based on refraction lens-based scanning [9] or micro-electromechanical systems (MEMS)-based scanning [10]. The main drawback of such techniques, besides only being able to address a single user [11] per time slot, is the rather low scanning speed and accuracy. Higher precision and speed can be achieved using a control method without mechanically moving parts, e.g., via phased arrays with either electronic [12] or optical phase shifting [13] between the elements of an antenna array. In the sub-THz range, due to the short wavelength, precise shifting of the phase to achieve high angular beam resolution is the key challenge as the complexity of the feed control increases. Implementing phase shifting with passive devices results in relatively high insertion losses [14],

The conceptualization of this work was done by J. Dittmer and A. Bhutani. The system-level experiments were conducted by J. Dittmer and F. Beuthan. The paper was written by J. Dittmer and revised and edited by A. Bhutani. L. Valenziano assembled the transmit antenna. S. Wagner and A. Tessmann provided the Rx module. The funding for this work was acquired by A. Bhutani, C. Koos, T. Zwick, and S. Randel.

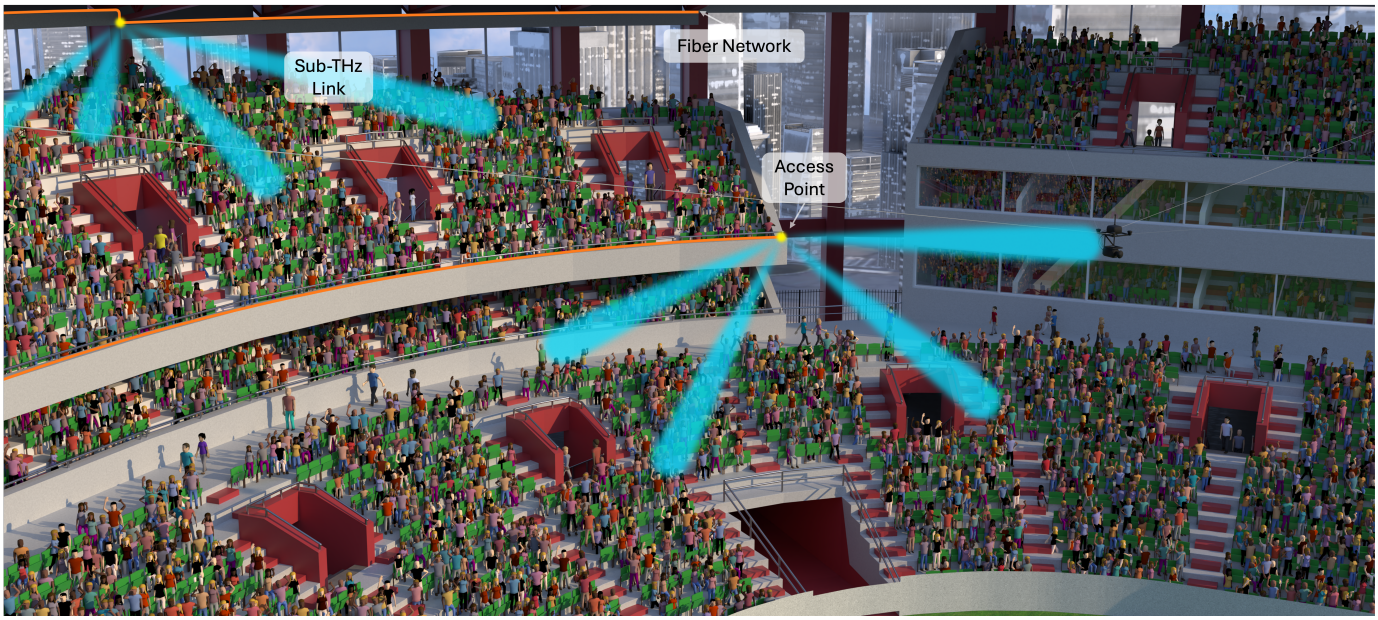

Fig. 1. Vision of future sub-THz wireless multi-user access networks. High-capacity sub-THz line-of-sight links connecting individual users to a single access unit are illustrated in a stadium environment. Each of these individual links provides ultra-broadband wireless connectivity through a fiber network backbone. The wireless links provide the flexibility to connect mobile and moving devices over a wireless channel. The sub-THz links are colored blue, whereas the fiber network is colored in orange.

while for active phase shifting, especially in miniaturized systems, thermal dissipation is most critical. Furthermore, digital beamforming can be used to serve multiple users with parallel data streams. However, digital beamforming faces challenges related to high circuit complexity and power consumption [11]. These challenges become even more pronounced in the sub-THz frequency range. In summary, the above concepts, such as phased array and digital beamforming, can be used to implement a P2MP link in the sub-THz range. However, due to the practical challenges associated with their implementation, there has been no system-level demonstration of a wireless link using these approaches to transmit data to multiple users simultaneously.

In contrast, frequency-based beam steering offers a simple yet cost-effective solution for achieving sub-THz wireless communication links for multiple users simultaneously. In this approach, a broadband signal is transmitted using a leaky-wave antenna (LWA), which allows a narrow beam to be steered in the desired direction by sweeping the carrier frequency [15]–[19]. As a result, multiple users can be served simultaneously by beams pointing in different directions, where each beam covers a portion of the total transmitter bandwidth. In [20] and [18], a $300\,\mathrm{GHz}$ LWA is used to demonstrate a beam-steering link for a single user. These works achieve data rates of up to $24\,\mathrm{Gbps}$ over a distance of $6\,\mathrm{cm}$ and $30\,\mathrm{Gbps}$ over $50\,\mathrm{cm}$, respectively. These short-distance P2MP links are demonstrated using a probe-contacted chip-based LWA assembly on an optical table, implying that the transmitter assembly is fragile and limited to a laboratory-based measurement setup. In contrast, this work presents the first system-level demonstration of a sub-THz multi-user link capable of operating at a significantly larger transmitter-to-receiver distance of 16 m. Unlike previous demonstrations, this work uses a robust split-block transmitter assembly with a standard rectangular waveguide WR3.4-based high-gain LWA and efficient digitally generated subcarriers for simultaneous data transmission to multiple users. This enables the first-ever long-distance sub-THz P2MP data transmission experiment at 16 m in a field test scenario, to the best of the authors' knowledge. We perform a proof-of-concept experiment using a wideband optoelectronic transmitter and two sub-THz electronic receivers, demonstrating long-haul wireless links in a single-user, a dual-user scenario, and evaluating link performance for up to four users. These measurements use QPSK and 16-QAM signaling schemes with different signal bandwidths. The signal-to-noise and distortion ratio (SNDR) is evaluated for all scenarios. In addition, measurements are performed with varying distances between the receiver units to investigate the smallest possible spacing between adjacent users in a real-life scenario. This analysis is critical to ensuring that each user's signal remains distinct and free of interference, thereby improving the overall efficiency and reliability of the communication link. In addition, the total number of users that can be served by a sub-THz wireless P2MP link was evaluated by demonstrating the simultaneous reception of individual data stream to one, two, three, and four spatially separated users.

The paper is organized as follows: Section II discusses application scenarios for sub-THz point-to-multipoint access points. In Section III, the receiver-specific data generation based on subcarriers is discussed. This is followed by an explanation of the optoelectronic transmitter and the characteristics of the LWA, and by an introduction of the all-electronic conversion concept and the wideband digital signal processing for each receiver. In Section IV, the measurement scenarios for a single-user link, a dual-user link, and up to four users are described. Individual user performance is evaluated based on SNDR for varying signal bandwidths and receiver unit spacings. Finally, a summary and an outlook of this work are presented in Section V.

II. Application Scenario of High-Speed Point-to-Multipoint sub-THz Links

As the 5th generation of wireless communication is used to provide full stadium coverage at sports events [22], [23], new ways of experiencing sports are explored in 6G research. Visitors to the stadium will be able to use augmented reality (AR) and virtual reality (VR) applications on 6G-enabled devices, as the technology can process larger amounts of data much faster than the prior generations of wireless communications. Channel capacity can be further increased by a factor of more than three with high-speed sub-THz networks, enabling data rates in the tens of gigabits per second and user in a multi-user scenario.

One potential application for short-range sub-THz access points is indoor home coverage. In this scenario, a single transmitter covers a small area, typically less than 2 meters, and serves a small number of users, typically between one and two, providing extremely high data rates, ideal for bandwidth-intensive applications such as holographic calls and AR/VR experiences. As the environment shifts to an office setting, the configuration adapts: the number of users per access point increases and the coverage area expands, with distances ranging from 2 to 5 meters, ensuring robust connectivity across a larger workspace. In educational environments, such as lecture halls, a similar setup is used. Here, the access point can support a larger number of users, typically spread over a distance of 5 to 10 meters, providing consistent performance for applications such as live-streaming lectures or interactive distance learning. For even larger venues, such as stadiums, more complex networks are required. Multiple sub-THz access points, each strategically placed and connected to a fiber backbone, work together to cover large areas. These access points can serve multiple users simultaneously within tens of meters. This vision is depicted in Fig. 1. One application of sub-THz access points for educational or stadium- based transmission is high-resolution, high-color-depth transmission of raw, uncompressed video from mobile cameras (e.g., spider-cam) to processing servers, enabling the accurate and seamless object-to-background separation required for 3D overlay and AR/VR content creation.

This paper evaluates a long-range, multi-user, sub-THz wireless link in a lecture hall environment, focusing on minimum user separation, maximum coverage within the beam steering range, user separability, and maximum allocable bandwidth per user.

III. Multi-User THz Link

To achieve broadband frequency coverage with high linearity and performance an optoelectronic transmitter was set up that transmits parallel data streams to multiple users. This allows easy integration into a fiber-based high-capacity communications network. In order to keep the receiver complexity as low as possible, an all-electronic intradyne coherent receiver per user is implemented in the multi-user communication link.

A. Optoelectronic Multi-User sub-THz Transmitter

The generation of sub-THz signals is based on optical and optoelectronic components. A leaky wave antenna is used for transmission, allowing simultaneous communication with multiple users. The optoelectronic and antenna hardware as well as the utilized digital signal processing (DSP) at the transmitter are described below.

1) Digital Subcarrier Generation for Multi-User Transmission: To generate individual data for each user to be transmitted simultaneously with a frequency-based beam steering antenna, individual frequency subcarriers must be generated. When an optoelectronic method is used to generate the transmit signal, two different approaches can be used to generate the user-specific subcarriers. The first option is to modulate

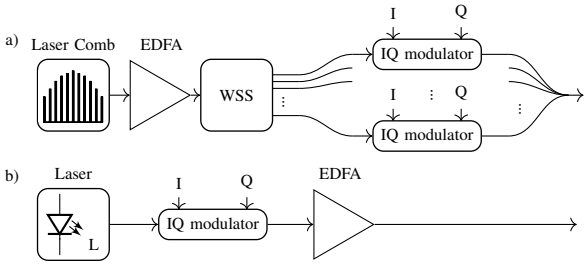

Fig. 2. Optical comb-based in a) and single carrier-based subcarrier generation principle in b). In the comb-based generation, individual comb lines are separated by a wavelength selective switch (WSS) and modulated separately before being combined. In the single carrier-based subcarrier generation, digital subcarriers are modulated using a single laser and modulator.

the baseband data of each user onto an individual optical carrier generated by either individual free-running lasers or laser-coherent frequency combs. This allows subcarriers to be generated over a wide frequency range (e.g., the entire IEEE-standardized [2] frequency band in the range of 253 to $322\,\mathrm{GHz}$) with multiple comparatively low-bandwidth electro-optical inphase and quadrature (IQ) modulators and digital-to-analog converters (DACs) that only require a bandwidth in the order of the maximum bandwidth allocated to each sub-THz user. This concept is depicted in Fig. 2a. The second, less complex and more flexible approach is to generate the subcarriers in the digital domain and modulate a single free-running laser with a high-bandwidth electro-optical IQ modulator through a high-bandwidth DAC. The basic setup for such an approach is shown in Fig. 2b and in Fig. 8. In this architecture, randomly generated binary information for each user is mapped to either four symbols, resulting in quadrature phase shift keying (QPSK), or 16 symbols, resulting in 16-quadrature amplitude modulation (16-QAM). This results in two or four bits per symbol, respectively. The user-specific symbol sequence is upsampled to a sampling rate of $120\,\mathrm{GSa/s}$ and filtered with a root-raised-cosine (RRC) filter with a spectral roll-off factor of $r = 0.1$, before being digitally frequency shifted to the corresponding subcarrier intermediate frequency. Figure 3 shows the baseband spectrum of four digitally generated subcarriers each with a symbol rate of $5\,\mathrm{GBd}$ and a spectral roll-off factor of 0.1. The choice of number of subcarriers and the signal bandwidth per user depends on the total receiver bandwidth and the maximum number of users. The receiver used in this work operates from $280\,\mathrm{GHz}$ to $320\,\mathrm{GHz}$ and hence has a maximum operation bandwidth of $40\,\mathrm{GHz}$. As seen in Fig. 3, the subcarriers for the four individual users will overlap when the symbol rate per

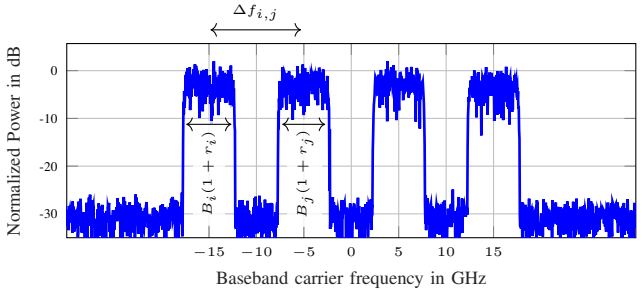

Fig. 3. Baseband spectrum of four subcarriers each with a signal bandwidth of 5 GBd and a spectral roll-off factor of 0.1.

user exceeds 10 GBd resulting in a leakage between users. If $\underline{s}_k[n]$ is the complex-valued discrete upsampled and filtered baseband transmit sequence for user k at sample point n, then

$$\underline{t}_k[n] = \underline{s}_k[n] \cdot \exp\left(\mathrm{j}2\pi n f_k / f_\mathrm{s}\right) \tag{1}$$

denotes the digital transmit signal of user k at the digital subcarrier center frequency f_k with respect to the sampling frequency f_s. The resulting transmit signal is generated by summing up all K subcarriers and normalizing the amplitude

$$\underline{t}[n] = \frac{1}{K} \sum_{k=0}^{K} \underline{t}_k[n]\,. \tag{2}$$

If the bandwidth per user is specified, the minimum subcarrier spacing must be chosen so that the individual spectra do not overlap in frequency. From a per-user symbol rate $B_{i,j}$ of the i^{th} and j^{th} user each with a roll-off factor of $r_{i,j}$, the minimum carrier spacing of

$$\Delta f_{i,j} = |f_i - f_j| \geq \frac{1}{2}\left(B_i\left(1+r_i\right) + B_j\left(1+r_j\right)\right)\,. \tag{3}$$

has to be fulfilled to prevent signal degradation. The subcarrier spacing is illustrated in Fig. 3.

2) Sub-THz Signal Generation by Optoelectronic Heterodyne Downconversion: The advantage of generating sub-THz signals by downconverting fiber-based optical signals using optoelectronic heterodyne detection in a broadband photodiode such as a uni-traveling carrier photodiode (UTC-PD) lies in the linear and broadband transfer characteristics of this detection scheme. The time-dependent output current $i(t)$ of a photodiode is directly proportional to the optical input power $P_{\text{opt.}}(t)$ via the responsivity $\mathcal{R}$ and thus is proportional to the squared magnitude of the optical field $E_{\text{opt.}}(t)$

$$i(t) \propto \mathcal{R} P_{\text{opt.}}(t) \propto \mathcal{R}|E_{\text{opt.}}(t)|^2\,. \tag{4}$$

If $E_{\text{opt.}}(t)$ consists of two individual frequencies, then $i(t)$ consists of the difference and the sum frequency. The sum frequency is inherently filtered out by the sub-THz electronic components, thereby resulting in a transmit signal with higher spectral purity. In our experimental setup, one of the individual laser frequencies is modulated using an electro-optical IQ modulator (Fujitsu FTM7992HM) with a 3-dB modulation bandwidth of 60 GHz. After digitally generating subcarrier IQ signals for each user as described in Section III-A1, the digital signal is converted to an electrical signal by a high-speed DAC in an arbitrary waveform generator (AWG, Keysight M8194A) at a sampling rate of 120 GSa/s and used as a drive signal for the IQ modulator. The modulated optical carrier is amplified to 23 dBm using an Erbium-doped fiber amplifier (EDFA, Connet 50C25). In order to reduce the out-of-band amplified spontaneous emission (ASE) noise generated by the EDFA, an optical bandpass filter with a bandwidth of 0.6 nm (i.e., 75 GHz) is used. To downconvert the optical signal to sub-THz frequencies, it is optoelectronically mixed in a UTC-PD (NTT/NEL J-Band Mixer) with the second laser having a frequency offset of approximately 300 GHz [24]. This results in a sub-THz carrier frequency of 300 GHz. To set the input power of the UTC-PD to the optimal value of approximately 11 dBm, a variable optical attenuator (VOA, Keysight N7764A) is used. The generated sub-THz signal is further amplified by a medium power amplifier (MPA, Fraunhofer IAF M155AMPH) with a small signal gain of 15 dB before being coupled to a frequency-based beam steering leaky-wave antenna to transmit data to multiple users simultaneously. The transmitter setup is depicted in Fig. 8.

3) Transmit Leaky-Wave Antenna Properties: The optoelectronically generated multi-user sub-THz signal is transmitted using an LWA. An LWA allows the transmit beam to be steered in the spatial domain as the operating frequency sweeps through the sub-THz range. As a result, multiple users located at different points within the coverage area can receive an independent beam simultaneously. The concept of frequency beam steering is a simple yet cost-effective beam steering method compared to phased array and digital beamforming approaches, especially in the sub-THz range, as described in the introduction. In order to establish a multi-user sub-THz long-distance wireless link based on the frequency beam steering method, two key constraints are considered in this work. First, the maximum signal bandwidth that can be allocated to each user is limited by the half-power beamwidth of the LWA and the spatial proximity of adjacent users. Second, the maximum distance between two users at the extreme ends of the coverage area, is determined by the transmitter-to-receiver distance and the beam steering range of the LWA.

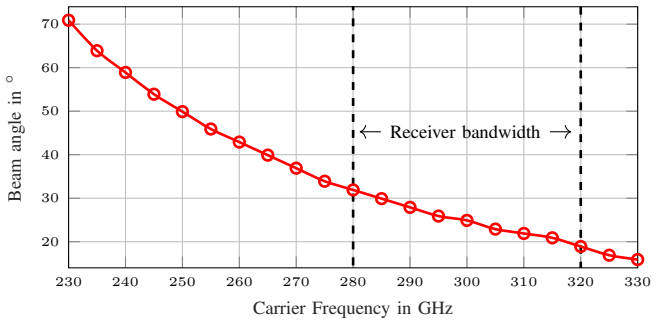

Fig. 4. Prototype leaky wave antenna radiation/reception measured beam angle characteristics as a function of the carrier frequency [25].

A conformal lens-integrated sub-THz LWA operating in the WR3.4 frequency band presented in [25] is used in this work. This LWA consists of an array of slots incorporated into a standard WR3.4 rectangular waveguide. This allows the transmitted beam to be steered from 71° to 16° relative to the broadside direction (0°) as the frequency sweeps from 230 to 330 GHz, respectively. The peak antenna gain is increased to

27 - 30 dBi by integrating a polytetrafluoroethylene (PTFE) based conformal plano-convex parabolic lens onto the LWA. The WR3.4 waveguide based LWA with the integrated lens is shown in Fig. 6. To transmit or receive data using an

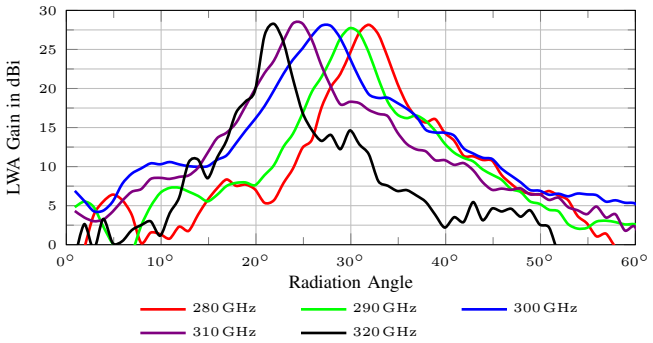

Fig. 5. Measured radiation pattern of the transmit leaky-wave antenna in the beam-steering plane at frequencies of 280 GHz, 290 GHz, 300 GHz, 310 GHz, and 320 GHz [25].

LWA, the individual users must be distributed in frequency according to the frequency-dependent radiation/reception characteristics of the given antenna. For the sub-THz WR3.4 antenna, the frequency-dependent radiation/reception angle is given in Fig. 4. In Fig. 5, the measured radiation pattern of the leaky-wave antenna in the beam-steering plane is shown at frequencies of 280 GHz, 290 GHz, 300 GHz, 310 GHz, and 320 GHz, which correspond to the maximum operating bandwidth of the receiver used in this work. The P2MP transmitter using digital subcarrier generation is limited by the maximum optical modulation bandwidth of 60 GHz. In this range, the antenna's half-power beamwidth (HPBW) is approximately 10 GHz, resulting in a maximum flat signal bandwidth of 10 GHz.

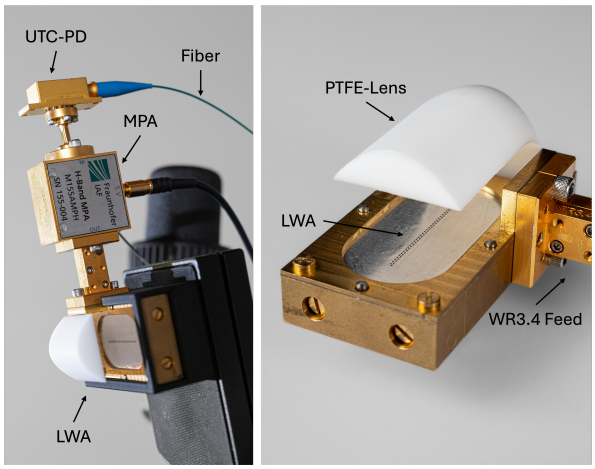

Fig. 6. Leaky wave antenna (LWA) integrated with PTFE based conformal plano-convex parabolic lens [25] (right) combined with medium power amplifier (MPA) for sub-THz frequencies feed by a uni-traveling-carrier photodiode (UTC-PD) (left).

B. All-Electronic sub-THz Receiver

Each user in the multi-user link is based on an all-electronic sub-THz signal downconversion. Advanced blind digital signal processing compensates for transmitter, receiver, and channel impairments. The receiver components and the DSP algorithms are described in the following.

1) Electronic sub-THz Down-Conversion: An all-electronic receiver with a WR 3.4 horn antenna and a spherical plano-convex PTFE lens was used for each individual user. The receiver is based on a packaged "InGaAs mHEMT MMIC" provided by the Fraunhofer Institute for Applied Solid State Physics IAF [26]. The purpose of the receiver is to convert the sub-THz signal from the frequency range of 280 to 320 GHz directly into complex baseband by tuning the local oscillator frequency $f_{1,2} = (280...320\,\mathrm{GHz})/36$ accordingly. The receiver module consists of a frequency tripler, an IQ demodulator and a sub-THz low noise amplifier (LNA). The MMIC module is fed by a $(280...320\,\mathrm{GHz})/3$ reference tone generated by a $\times 12$ frequency multiplier [27] and a low-frequency synthesizer. A isolator is used to prevent back reflections into the frequency multiplier causing unwanted frequency drifts and harmonics. The baseband signals are pre-amplified by two broadband RF amplifiers (SHF 827A) and sampled by two channels of a 32 GHz real-time oscilloscope (Keysight DSOZ334A) at a sampling rate of $80\,\mathrm{GSa/s}$. The receiver setup for a single receiver, including the real-time oscilloscope and the synthesizer to generate the down-conversion reference tone is shown in Fig. 7 and a schematic of the receiver setup is depicted in Fig. 8. In comparison to the highest achievable transmit bandwidth of 60 GHz around 300 GHz the maximum link bandwidth is limited by the individual receivers, which have a two-sided bandwidth of 40 GHz [26]. This results in a maximum demonstrable angular coverage of 12° (from 19° to 31°) as depicted in Fig. 4.

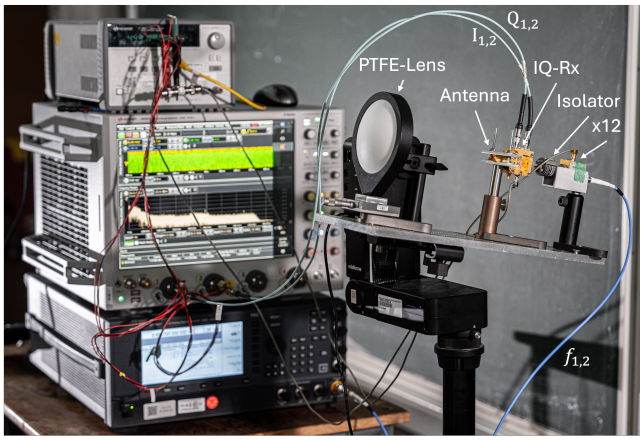

Fig. 7. All-electronic sub-THz receiver consisting of a PTFE-lens, a standard WR3.4 horn antenna, a sub-THz IQ receiver, an isolator, and a local oscillator generated using a $\times 12$ multiplier. The synthesizer generating the clock and the oscilloscope are depicted on the left.

2) Broadband Multi-User sub-THz Digital Signal Processing: The simultaneously transmitted signals for all users are separately captured for each user at a sampling rate of $80\,\mathrm{GSa/s}$ with a memory length of 2^{23} samples and are processed offline with fully blind (i.e. no preamble is used) broadband signal processing adapted from optical communications. In a first step, the signal is digitally filtered to suppress noise and interference from neighboring users, and then resampled to two samples per symbol. A feedforward timing recovery algorithm based on the approach of Barton and Al-Jalili [28], [29] is used to estimate and correct residual

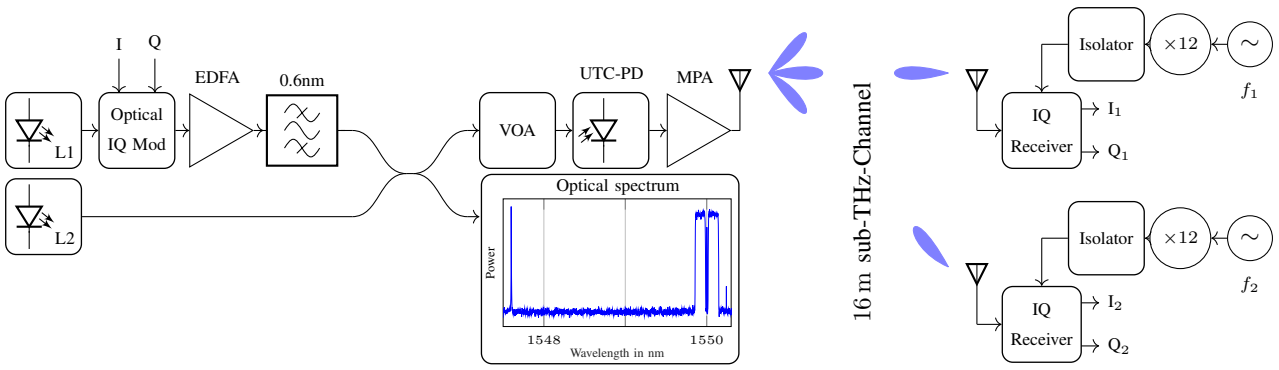

Fig. 8. Multi-user sub-THz transmitter based on optoelectronic heterodyning in a uni-traveling-carrier photodiode (UTC-PD). Complex baseband data (Inphase: I and Quadrature: Q) containing digital sub-carriers for each user is modulated on a first laser (L1) using an optoelectronic IQ modulator. The resulting signal is amplified with an Erbium-doped fiber amplifier (EDFA) and combined with the a second laser (L2) in a 3-dB coupler for optoelectronic heterodyne detection. The frequency difference between L1 and L2 is equal to the resulting sub-THz center carrier frequency. An optical bandpass filter suppresses out-of-band amplified spontaneous emission noise generated by the EDFA. A variable optical attenuator (VOA) is used to optimize the input power to the UTC-PD. The sub-THz signal is further amplified by a medium power amplifier (MPA) before getting transmitted by the leaky-wave antenna (LWA). The optical spectrum for two 15-GBd users/sub-carriers is indicated in the inset. The receivers consist of a local oscillator at a frequency from $f_{1,2} = 7.77$ to $8.88\,\mathrm{GHz}$, which is upconverted by a factor of 12 to a frequency of 93.333 to 106.66 GHz and in the coherent IQ receiver again by a factor of 3 to a frequency in the range of 280 to 320 GHz. The sub-THz signals are received with a WR3.4 horn antenna and pre-focused by a polytetrafluorethylen (PTFE) lens and downconverted to baseband with the 280 to 320 GHz local oscillator in the all-electronic IQ receivers.

clock frequency and phase offsets between the transmitter and the individual receivers. Next, an adaptive receive filter consisting of a time-domain linear equalizer (TDE) with 51 half-symbol-spaced taps is used. A single output sample is generated for each symbol, and the equalizer coefficients are blindly adjusted using the constant modulus algorithm (CMA). The CMA, a blind stochastic gradient algorithm, aims to minimize the radial error of the equalizer output [30] and is therefore not impaired by phase noise and frequency offset. To estimate and compensate for the frequency offset between the transmit and receive oscillators, we use the algorithm described in [31]. First, the received samples are raised to the fourth power to eliminate the modulation. This result is then multiplied by its delayed and conjugated form. The product is then averaged over M symbols to reduce noise. Finally, the frequency offset is calculated by taking the argument of the averaged result and dividing it by four. Especially when using optoelectronic sub-THz signal generation, it is important to compensate for the frequency drifts resulting from the higher frequency fluctuations between the signal and the reference lasers. The residual phase error caused by the phase noise of the electrical and optical oscillators is corrected using the Viterbi-Viterbi algorithm [32]. This involves raising the symbols to the fourth power and averaging the resulting phase error over $M = 129$ symbols. After phase unwrapping, a delayed version of the received symbols is used to correct the phase error. To compensate for the residual imbalance and skew between the inphase and quadrature components introduced by the transmitter, we use a symbol-spaced real-valued 2x2 multiple-input multiple-output (MIMO) post-equalizer with 21 taps. The coefficients of this equalizer are adapted using the decision-directed least-mean-squares (LMS) algorithm [33]. The performance of each link is evaluated by applying hard decisions to the received symbols and comparing them to each user's transmitted sequence to calculate the SNDR and bit-error ratio (BER) per user. Although these algorithms were originally developed for single-radius rotationally symmetric constellations such as QPSK, they have also shown reasonably good performance with multi-radial constellations such as 16-QAM.

IV. Sub-THz Multi-User Transmission Results

The transmission and reception of multi-user sub-THz signals, utilizing digital subcarriers with an optoelectronic transmitter and an all-electronic receiver, enable effective communication in the frequency range from 280 GHz to 320 GHz, limited by the receiver's bandwidth [27]. As shown in Fig. 4, an angular coverage of 12° can be achieved in this range given the frequency beam steering characteristics of the LWA. A sub-THz multi-user link with a transmitter to receiver distance of 16 m is established in a lecture hall as shown in Fig. 9. First, a single-user transmission is considered, followed by dual-user and multi-user transmission scenarios. The transmitter and receiver architectures are explained in Sections III-A and III-B, respectively.

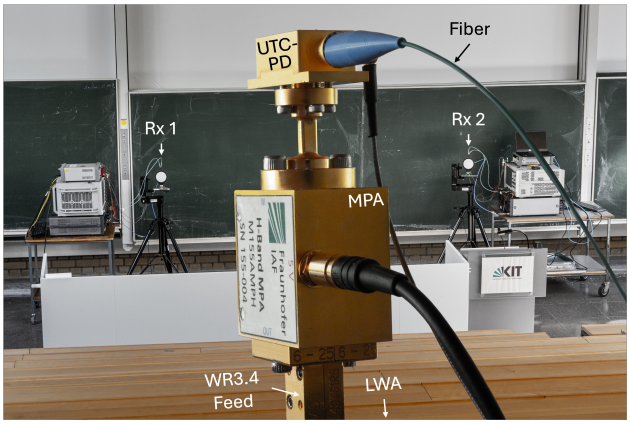

Fig. 9. Lecture-hall 16-m transmission setup. Two all-electronic sub-THz receivers (Rx1 & Rx2) and the optoelectronically assisted multi-user transmitter consisting of uni-travelling-carrier photodiode (UTC-PD) and medium power amplifier (MPA) are shown.

A. High Capacity Single User Transmission

To evaluate the maximum channel capacity provided by the optoelectronic transmitter and the all-electronic receiver, a single-user transmission link is set up. In this case, all transmit power is radiated in one spatial direction, resulting in the highest received power per user and the maximum achievable SNDR. In this case, limited by the antenna's half-power beamwidth (HPBW), a single user operating at a subcarrier frequency of 300 GHz decodes a symbol rate of 20 GBd for both QPSK and 16-QAM schemes with a BER of less than 2.4×10^{-2}, which can still be compensated using soft decision forward error correction coding (SD-FEC) with a 20% coding overhead, e.g., with low-density-parity-check (LDPC) codes [34], [35]. This results in a maximum data rate of 40 Gbps for QPSK and 80 Gbps for 16-QAM over the 16-m indoor lecture-hall link. To the best of the authors' knowledge, this is the highest data rate achieved in a sub-THz beam steering link to date. The constellation diagrams for QPSK and 16-QAM are given in Fig. 10. For QPSK, the resulting SNDR performance is 15.2 dB with a measured BER of $5.15 \cdot 10^{-7}$ and 14.3 dB with a measured BER of $1 \cdot 10^{-2}$ for 16-QAM.

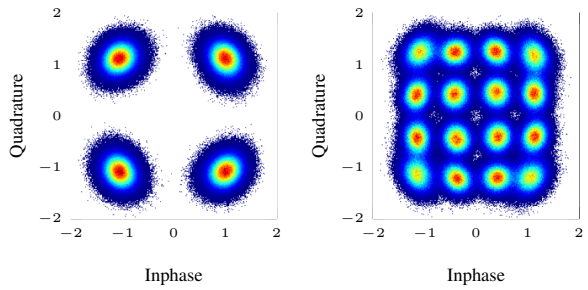

Fig. 10. Received constellations for single-user 20-GBd transmission at a subcarrier frequency of 300 GHz resulting in bit rates of 40 Gbps for QPSK and 80 Gbps for 16-QAM. The measured BER is $5.15 \cdot 10^{-7}$ and $1 \cdot 10^{-2}$, respectively.

B. Simultaneous Dual-User Link

To investigate the influence of data rate and subcarrier spacing on the multi-user communication link, a dual-user transmission is set up over the 16 m link. Fig. 11 shows five users, U1 to U5, operating at frequency subcarriers of 280 GHz, 290 GHz, 300 GHz, 310 GHz, and 300 GHz, respectively. The spacing between these users and the distance

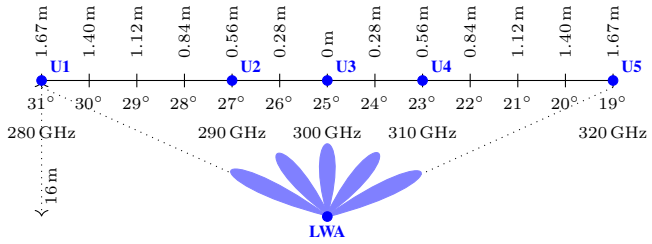

Fig. 11. Location of individual users (U) in angle and distance (not to scale) compared to each other and the leaky-wave antenna (LWA) frequency-based beam-steering transmitter.

between the transmitting LWA and each of these users are also shown in the figure. The wideband LWA is capable of transmitting beams to all users simultaneously. The minimum distance between any two users (e.g., U2 and U3 or U3 and U4) is 0.56 m and the maximum distance between the users U1 and U5 is 3.34 m. Table I shows the suppression between the primary and secondary radiation lobes corresponding to users U1 through U5. The primary user refers to the user intended to receive the radiated signal, while the secondary user refers to one not intended to receive the radiated signal. The isolation values between individual users, as indicated in this table, are obtained by analyzing the radiation pattern of the transmit LWA at 280 GHz, 290 GHz, 300 GHz, 310 GHz, and 320 GHz as shown in Fig. 5. As seen in the table, the lowest isolation is observed between adjacent users, e.g., the isolation between primary U2 (27° at 290 GHz) and secondary U1 (31° at 280 GHz) is 3.3 dB, while the best isolation is observed between users on the extreme ends, e.g., primary U5 (19° at 320 GHz) and secondary U1 (31° at 280 GHz) show an isolation of 22.6 dB. The isolation between adjacent users can be improved by modifying the radiation characteristics of the transmit LWA such that the suppression between its radiation lobes is higher. However, this would, in turn, imply that the HPBW of the radiation lobes will decrease, which would restrict the signal bandwidth per user. Hence, there is a fundamental trade-off between the signal bandwidth per user and the isolation between adjacent users that can be achieved with a frequency-based beam-steering transmitter frontend. Compared to the single-user transmission, the received power

TABLE I
SUPPRESSION BETWEEN THE PRIMARY AND SECONDARY RADIATION LOBES CORRESPONDING TO USERS U1 THROUGH U5.

Secondary \ Primary	U1	U2	U3	U4	U5
U1	-	3.3 dB	10.6 dB	18.6 dB	22.6 dB
U2	3.6 dB	-	6.7 dB	14.1 dB	18.1 dB
U3	8.9 dB	3.9 dB	-	4.7 dB	9.5 dB
U4	10.9 dB	9.5 dB	5.2 dB	-	4.7 dB
U5	16.6 dB	13.1 dB	14.8 dB	7.1 dB	-

per user and thus the SNDR is reduced by 3 dB if both beams have equal power. This is further discussed in Section IV-C. For simplicity, the data rate and modulation format transmitted per user is kept constant for all users in a single measurement. Optimization of link performance could be achieved by dynamic allocation of bandwidth and modulation format per user. The transmission performance for each of these dual-user combinations is evaluated by varying the the symbol rate $B_i = B_j$ from 5, 10 to 15 GBd. The results are shown in Fig. 12 for QPSK modulation and in Fig. 13 for 16-QAM. Four different dual-user scenarios are evaluated for both modulation formats. To evaluate the overall performance of a dual-user link, the two sub-THz receiver units are placed at U1 and U3, operating at frequency subcarriers of 280 GHz and 300 GHz, respectively, and located at angles of 31° and 25°, respectively, with respect to the broadside direction of the LWA (see Fig. 11). Thereafter, two link measurements, using (U2 and U3) and (U3 and U4), are performed, in which the two receiver units are moved closer to each other both in the spatial and frequency domains. In these latter two measurements, the frequency subcarrier spacing is reduced to $\Delta f_{2,3} = \Delta f_{3,4} = 10$ GHz, and the angular spacing in the

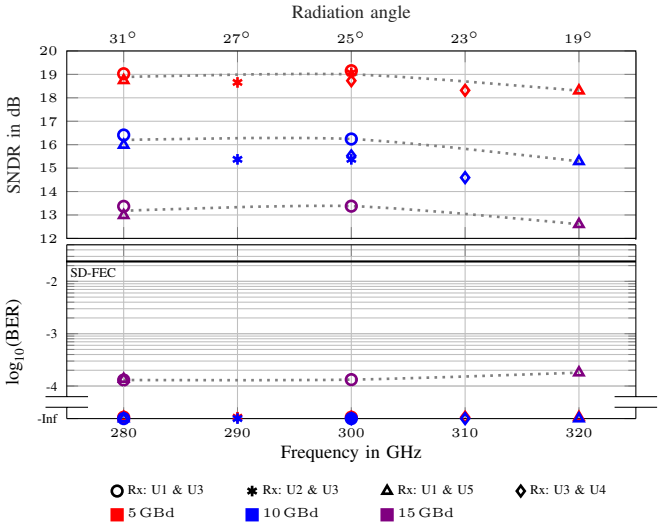

Fig. 12. Dual-user transmission performance for four individual receiver location scenarios (Rx: U1 & U3, Rx: U2 & U3, Rx: U1 & U5, Rx: U3 & U4) with each three different data rates (5, 10, and 15 GHz) for **QPSK** modulation.

spatial domain is reduced to only 2°. In this arrangement, the effect of overlapping spectra can be evaluated for both users since the subcarrier spacing is below the limit given in Eq. 3. To demonstrate the maximum angular coverage achieved by the receiver modules, a dual-link measurement is performed by placing the receiver units at U1 and U5. As shown in Fig. 11, U1 and U5 are located at angles of 31° and 19°, respectively, with respect to the broadside direction of the LWA, and their subcarrier frequencies (280 GHz and 320 GHz, respectively) have a spacing of $\Delta f_{1,5} = 40\,\text{GHz}$. The large subcarrier

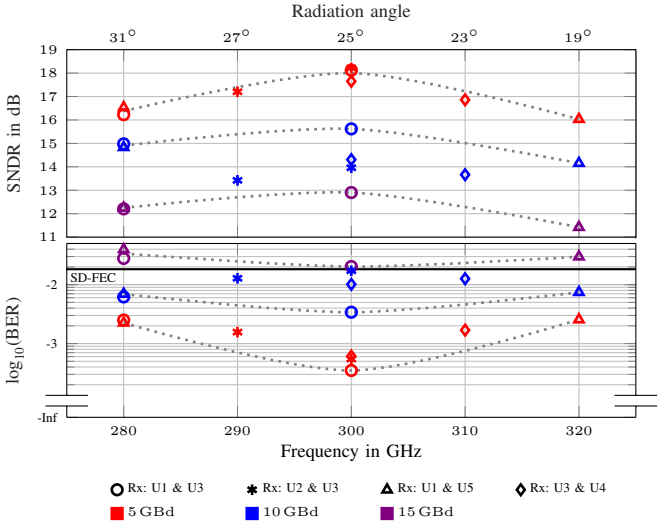

Fig. 13. Dual-user transmission performance for four individual receiver location scenarios (Rx: U1 & U3, Rx: U2 & U3, Rx: U1 & U5, Rx: U3 & U4) with each three different data rates (5, 10, and 15 GHz) for **16-QAM** modulation.

spacing enables an investigation of the antenna radiation pattern influence without disturbing neighboring subcarriers. All subcarrier spacings and signal bandwidths for all dual-user measurement scenarios are summarized in Table II. As indicated in the table, a total of 24 measurement scenarios were evaluated, including four dual-user combinations, each with three different symbol rates and two modulation formats (QPSK and 16-QAM). The scenarios where the subcarrier frequency spacing is less than the signal bandwidth (i.e. where Eq. 3 is not satisfied), resulting in signal degradation, are highlighted in blue in the table. The measurement results using

TABLE II
BANDWIDTH AND CARRIER SPACING FOR ALL DUAL-USER SCENARIOS.

	$\Delta f_{i,j} = \lvert f_i - f_j \rvert$	$B_{i,j}(1+r_{i,j})$		
		5 GBd	10 GBd	15 GBd
U1-U3	$\lvert 280 - 300 \rvert = 20\,\text{GHz}$	5.5 GHz	11 GHz	16.5 GHz
U2-U3	$\lvert 290 - 300 \rvert = 10\,\text{GHz}$	5.5 GHz	11 GHz	16.5 GHz
U1-U5	$\lvert 280 - 320 \rvert = 40\,\text{GHz}$	5.5 GHz	11 GHz	16.5 GHz
U3-U4	$\lvert 300 - 310 \rvert = 10\,\text{GHz}$	5.5 GHz	11 GHz	16.5 GHz

5, 10, and 15 GBd QPSK modulation are shown in Fig. 12. We observe that the performance is nearly constant for all user scenarios as long as the spectra of adjacent subcarriers do not overlap. The degradation in signal quality caused by this overlap can be observed for a subcarrier spacing of 10 GHz (e.g. user scenarion U2 and U3 or U3 and U4) and a symbol rate of 10 GBd, resulting in a signal bandwidth of $10\,\text{GBd}\,(1+r) = 11\,\text{GHz}$. Where $r = 0.1$ is the frequency roll-off of the pulse shaping filter. This results in a degradation of 0.5 to 1 dB compared to the non-overlapping transmission. Consequently, a 15 GBd signal with a bandwidth of 16.5 GHz can no longer be received at a subcarrier spacing of 10 GHz. Similarly, the measurement results for 5, 10, and 15 GBd 16-QAM are shown in Fig. 13. For 16-QAM, a slight SNDR degradation can be observed due to a lower conversion gain and higher nonlinearities of the receiver that cannot be compensated by the DSP. The degradation of signal quality towards the edge of the receiver bandwidth at 280 and 320 GHz can be explained by the higher nonlinearity and lower response of the transmitter amplifier, UTC-PD, and the lower sensitivity of the all-electronic receiver modules. The dual-user link achieved maximum data rates of 30 Gbps per user (60 Gbps total) for QPSK and 40 Gbps per user (80 Gbps total) for 16-QAM, with a BER limit of 2.4×10^{-2}, correctable with a 20% overhead SD-FEC. To the best of the authors' knowledge, this is the highest data rate achieved for a sub-THz dual-user link operating around 300 GHz over a distance of 16 m.

C. Per User Scaling Link Performance

A comparison of state-of-the-art sub-THz P2MP wireless links operating around 300 GHz is given Table III. To evaluate the performance degradation for an increasing number of users caused by a constant transmitted sub-THz power of approximately 0 dBm, the SNDR for a user (U3) located at 25° (300 GHz) is evaluated over an increasing number of transmitted user frequency bands resulting in a maximum coverage of 2.23 m between users U2 and U5 with a minimum user spacing of 0.56 m. To evaluate the SNDR performance of an increasing number of simultaneous users at data rates comparable to the dual-link scenario, either a 5 GBd QPSK or a 16-QAM signal is transmitted to each individual user. To avoid signal degradation from adjacent users, the subcarrier spacing is set to 10 GHz, resulting in a maximum of four simultaneous users. (Note that the receiver bandwidth is limited from 280 to 320 GHz. Therefore, considering a subcarrier spacing of 10 GHz limits this analysis to a maximum of four users). The corresponding users in the 16 m link are given in Fig. 11. For

TABLE III
POINT-TO-MULTIPOINT WIRELESS LINK EXPERIMENTS IN THE SUB-THZ RANGE.

Reference	**This Work**	[36]	[37]	[18]	[38]	[20]	[21]
Technology	Leaky-wave	Phased-array	Phased-array	Leaky-wave	Phased-array	Leaky-wave	2x2 MIMO
Center frequency	300 GHz	256 GHz	215 GHz	300 GHz	246 GHz	300 GHz	300 GHz
Tx to Rx distance	16 m	0.025 m	11.24 m	0.5 m	0.36 m	0.06 m	1.2 m
Number of users	up to 4	1	1	1	1	1	2
User spacing max|min	3.34 | 0.56 m	-	-	-	-	-	0.24 | 0.21 m
Max. data rate per user	80 Gbps	52 Gbps	32 Gbps	30 Gbps	32 Gbps	24 Gbps	64 Gbps

the single user link, only data is transmitted to U3. For the dual-user link the data is sent to U3 and U4. In the three-user link data is sent to U2, U3 and U4. Finally, for the four-user link, data is sent to U2, U3, U4 and U5. In this case, the sub-THz spectrum allocated to U2, U3, U4, and U5 is centered at 290 GHz, 300 GHz, 310 GHz, and 320 GHz, respectively, with each signal having a bandwidth $B_{2,3,4,5}(1 + r_{2,3,4,5})$ of 5.5 GHz, corresponding to a symbol rate of 5 GBd and a spectral roll-off factor of 0.1. Since the number of receiver hardware units available in this work is limited to two, the received data is analyzed for the most challenging scenario involving the middle two adjacent users, U3 and U4, as they are most susceptible to crosstalk from their neighboring users. The resulting received per-user SNDR for U3 at 300 GHz and U4 at 310 GHz for up to four simultaneous transmitted users in the sub-THz multi-user link is shown in Fig. 14. The theoretical SNDR degradation is determined by assuming an ideal 3 dB drop in SNDR for every doubling of the number of users. This model is fitted to the measured SNDR curve. As in the dual-user link, the performance of U4 is lower than U3, mainly due to the lower receiver performance at 310 GHz [27]. Since the average optical power remains constant, the

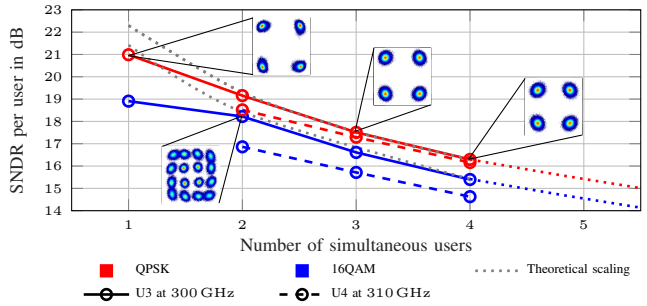

Fig. 14. Signal-to-noise-and distortion ratio (SNDR) scaling for an increasing number of simultaneously transmitted user (U2 to U5) signals with a symbol rate of 5 GBd and QPSK/16-QAM modulation. The data is evaluated for two adjacent users U3 (25°, 300 GHz) and U4 (23°, 310 GHz).

per-user power degrades as the number of users increases. Since the sub-THz power is held constant, the optical power degradation per user is proportional to the sub-THz receive power degradation for an individual user. For a transmit power of 0 dBm (without LWA gain), the receive power for a single user is measured to be approximately −32 dBm. Doubling the number of users results in −35.1 dBm per user. For three and four users, the receive power per user is −36.3 dBm and −37.8 dBm, respectively. Therefore, it can be observed that if the transmit power is kept constant, the received power and thus the resulting SNDR per user in a linear system degrades by 3 dB when the number of users is doubled. This trend can be observed in the SNDR and receive power measurements as the number of users increases from two to four for both modulation schemes. In Fig. 14, the SNDR decreases by 2.9 dB as the number of users increases from two to four. Note that due to nonlinearities caused by the sub-THz receiver and transmitter, the SNDR drop is less than 3 dB as the number of users increases from one to two. Since the receive power for a single receiver is above the optimal operating point of about −35 dBm [27], the SNDR improvement around 1.8 dB for QPSK and 0.8 dB for 16-QAM. As 16-QAM is more susceptible to nonlinear distortion, the SNDR degradation is 1 dB higher. Except for the single user scenario, the measured SNDR per user follows the theoretical trend very closely. To the best of the authors' knowledge, this multi-user link demonstrates the first simultaneous transmission of 10 Gbps (QPSK) and 20 Gbps (16-QAM) per user for up to four users. This results in a total maximum data rate of $4 \cdot 20\,\text{Gbps} = 80\,\text{Gbps}$ over an angular range of 8° (subcarriers at 290, 300, 310, and 320 GHz for four users) over a distance of 16 m. Based on an extrapolation of the theoretical curve shown in Fig. 14, the maximum number of users that can be supported while maintaining a measured pre-FEC BER below 2.4×10^{-2} is 5 for 16-QAM modulation. For QPSK modulation, which is more robust to noise and interference, the system can support up to 9 users under the same conditions of the 16 m link.

V. SUMMERY AND FUTURE OUTLOOK

This paper demonstrates the first sub-THz multi-user wireless link operating over a distance of several meters, showing its potential for future sub-THz access points. An optoelectronic transmitter is used in which a free-running laser and an electro-optic IQ modulator provide frequency subcarriers for multiple users. A UTC-PD converts the optical signal to the sub-THz range. The sub-THz signal is transmitted by a conformal lens-integrated rectangular waveguide (WR3.4) leaky-wave antenna to spatially separated users. Each user is assigned a specific frequency subcarrier and the total signal bandwidth is divided among the number of users. At the receiver end, a multi-user setup is implemented using two units of an all-electronic broadband sub-THz receiver operating from 280 to 320 GHz. Sub-THz wireless link measurements are performed in a lecture hall environment with a transmitter-to-receiver distance of 16 m using QPSK and 16-QAM schemes. In the single-user measurement, a data rate of 80 Gbps is achieved with a measured BER of $1.04 \cdot 10^{-2}$. In the dual-user measurement, with the users separated by a distance of 3.4 m, a per-user data rate of 40 Gbps is obtained with a BER of $3.1 \cdot 10^{-3}$. In both cases, blind feedforward DSP is used separately at each receiver. To the

best of the authors' knowledge, these are the highest data rates demonstrated to date for a point-to-multipoint sub-THz link at carrier frequencies around $300\,\mathrm{GHz}$. The performance of the sub-THz point-to-multipoint link has been scaled up to 4 users by analyzing the performance of the SNDR over multiple users. The multi-user scenario results in a minimum distance of $0.56\,\mathrm{m}$ between two adjacent users at data rates of up to $40\,\mathrm{Gbps}$. In future, high-data-rate sub-THz point-to-multipoint links could be used for 6G use cases, such as uncompressed live broadcasting of video content with full stadium coverage. This work presents proof-of-concept experiments using split-block components for system-based link evaluation. The future vision for handheld mobile devices requires a miniaturized receiver integrated with an MMIC and a planar antenna. To increase the sub-THz output power, a power amplifier with higher saturated output can be added to the transmitter, or an adapted transmit LWA with a conformal lens can be used to achieve even higher antenna gains and higher equivalent isotropically radiated power (EIRP). Additionally, the sensitivity of the receiver can be improved, for example, by using a receiver MMIC with a lower noise figure and conversion loss. Proof-of-concept experiments demonstrated in this paper show simultaneous transmission to up to four individual users, resulting in a total data rate of $80\,\mathrm{Gbps}$. A comparison to other sub-THz P2MP experiments is given in TAB. III. The concept of a sub-THz P2MP link, as shown in this paper, can be seamlessly integrated into a fiber-optic network using mature optical and optoelectronic components for broadband signal generation. This will serve as a guideline for developing future concepts and design considerations related to high-capacity sixth-generation sub-THz mobile networks.

ACKNOWLEDGMENT

This work is supported by the BMBF projects Open6GHub (Grant 16KISK010) and by the European Research Council (ERC Consolidator Grant 'TeraSHAPE', #773248). We thank Hannes Hohn for the graphical design and Luiz Dittmer for the setup and component pictures.

REFERENCES

[1] CISCO, "Cisco Visual Networking Index (VNI) Update Global Mobile Data Traffic Forecast," White Paper ,2017.

[2] V. Petrov et al., "IEEE 802.15.3d: First Standardization Efforts for Sub-Terahertz Band Communications toward 6G," in IEEE Communications Magazine, vol. 58, no. 11, pp. 28-33, 2020.

[3] NIST/SEMATECH "e-Handbook of Statistical Methods," http://www.itl.nist.gov/div898/handbook/, 2022.

[4] K. Sano et al., "Ultra-fast optoelectronic circuit using resonant tunnelling diodes and uni-travelling-carrier photodiode," in Electronics Letters, 1998, 34(2):215.

[5] H. Hamada et al., "Millimeter-wave InP Device Technologies for Ultra-high Speed Wireless Communications toward Beyond 5G," 2019 IEEE International Electron Devices Meeting (IEDM), pp. 9.2.1-9.2.4, 2019.

[6] I. Kallfass, et al., "64 Gbit/s Transmis- sion over 850 m Fixed Wireless Link at 240 GHz Carrier Frequency, " in Journal of Infrared, Millimeter, and Terahertz Waves 36, 221–233, 2015.

[7] H. Hamada et al., "300-GHz-Band 120-Gb/s Wireless Front-End Based on InP-HEMT PAs and Mixers," in IEEE Journal of Solid- State Circuits, vol. 55, no. 9, pp. 2316-2335, 2020.

[8] J. Dittmer et al., "200 Gbit/s Wireless THz Transmission over 52m using Optoelectronic Signal Generation," 2023 53rd European Microwave Conference (EuMC), pp. 134-137, 2023.

[9] M. Alonso-delPino et al., "Beam Scanning of Silicon Lens Antennas Using Integrated Piezomotors at Submillimeter Wavelengths," in IEEE Transactions on Terahertz Science and Technology, vol. 9, no. 1, pp. 47-54, 2019.

[10] X. Liu et al., "Terahertz Beam Steering Concept Based on a MEMS-Reconfigurable Reflection Grating," Sensors 10, 2874, 2020.

[11] X. J. Fuet al., "Terahertz Beam Steering Technologies: From Phased Arrays to Field-Programmable Metasurfaces". Advanced Optical Materials vol. 8, 1900628, 2020.

[12] Y. Yang, O. D. Gurbuz and G. M. Rebeiz, "An Eight-Element 370–410-GHz Phased-Array Transmitter in 45-nm CMOS SOI With Peak EIRP of 8–8.5 dBm," in IEEE Transactions on Microwave Theory and Techniques, vol. 64, no. 12, pp. 4241-4249, 2016.

[13] P. Lu et al., "Photonic Assisted Beam Steering for Millimeter-Wave and THz Antennas," 2018 IEEE Conference on Antenna Measurements & Applications (CAMA), pp. 1-4, 2018.

[14] D. Müller et al., "A h-band reflective-type phase shifter MMIC for ISM-Band applications," 2014 IEEE MTT-S International Mi- crowave Symposium (IMS2014), pp. 1-4, 2014.

[15] P. Lu et al., "InP-Based THz Beam Steering Leaky-Wave Antenna," in IEEE Transactions on Terahertz Science and Technology, vol. 11, no. 2, pp. 218-230, 2021.

[16] K. Sarabandi et al., "A Novel Frequency Beam-Steering Antenna Array for Submillimeter-Wave Applications," in IEEE Transactions on Terahertz Science and Technology, vol. 8, no. 6, pp. 654-665, 2018.

[17] K. Murano et al., "Low-Profile Terahertz Radar Based on Broadband Leaky-Wave Beam Steering," in IEEE Transactions on Terahertz Science and Technology, vol. 7, no. 1, pp. 60-69, 2017.

[18] J. Tebart et al., "Mobile 6G Communications at THz Frequencies Enabled by Leaky-wave Antenna Beam Steering," 2023 53rd European Microwave Conference (EuMC), pp. 142-145, 2023.

[19] T. Haddad et al., "THz Optoelectronic 2-D Beam Steering Transmitter for Short-Range Communications," 2024 15th German Microwave Conference (GeMiC), pp. 300-303, 2024.

[20] P. Lu et al., "Mobile THz Communications using Photonic Assisted Beam Steering Leaky-Wave Antennas," Opt. Express, vol. 29, 2021.

[21] O. Stiewe et al., "Towards High-Capacity THz-Wireless P2MP Communication Systems for 6G," 2022 52nd European Microwave Conference (EuMC), pp. 40-43, 2022.

[22] I. Kanno, "Trends and Use Cases of 5G," in Policies and Challenges of the Broadband Ecosystem in Japan. Advances in Information and Communication Research, vol 4. Springer, 2022.

[23] M. E. Diago-Mosquera and M. Rodriguez, "Two-Frequency mmWave Measurement-Based Modeling for Stadium Coverage," 4th URSI Atlantic Radio Science Meeting (AT-RASC), pp. 1-3, 2024.

[24] T. Harter et al., "110-m THz Wireless Transmission at 100 Gbit/s Using a Kramers-Kronig Schottky Barrier Diode Receiver," 2018 European Conference on Optical Communication (ECOC), pp. 1-3, 2018.

[25] A. Bhutani et al., "Sub-THz Conformal Lens Integrated WR3.4 Antenna for High-Gain Beam-Steering," in IEEE Open Journal of Antennas and Propagation, 2024.

[26] I. Kallfass et al., "Towards MMIC-Based 300GHz Indoor Wireless Communication Systems," IEICE Transactions on Electronics 98.12, 1081-1090, 2015.

[27] I. Kallfass et al., "MMIC chipset for 300 GHz indoor wireless communication," 2015 IEEE International Conference on Microwaves, Communications, Antennas and Electronic Systems (COMCAS), pp. 1-4, 2015.

[28] S. K. Barton and Y. O. Al-Jalili, "A symbol timing recovery scheme based on spectral redundancy," IEE Colloquium on Advanced Modulation and Coding Techniques for Satellite Communications, pp. 3/1-3/6, 1992.

[29] P. Matalla et al., "Hardware Comparison of Feed-Forward Clock Recovery Algorithms for Optical Communications," 2021 Optical Fiber Communications Conference and Exhibition (OFC), pp. 1-3, 2021.

[30] S. Moshirian et al., "Blind channel equalization," arXiv preprint arXiv:1208.2205, 2012.

[31] A. Leven et al., "Frequency Estimation in Intradyne Reception," in IEEE Photonics Technology Letters, vol. 19, no. 6, pp. 366-368, 2007.

[32] Andrew J. Viterbi and Audrey M. Viterbi, "Nonlinear estimation of PSK-modulated carrier phase with application to burst digital transmission," in IEEE Transactions on Information Theory, vol. 29, no. 4, pp. 543-551, 1983.

[33] S. Randel et al., "All-electronic flexibly programmable 864-Gb/s single-carrier PDM-64-QAM," in Optical Fiber Communication Conference: Postdeadline Papers, (Optica Publishing Group, 2014), paper Th5C.8., 2014.

[34] A. Leven and L. Schmalen, "Status and Recent Advances on Forward Error Correction Technologies for Lightwave Systems," in Journal of Lightwave Technology 32, 2735-2750 , 2014.
[35] D. A. Morero et al., "Non-Concatenated FEC Codes for Ultra-High Speed Optical Transport Networks," in 2011 IEEE Global Telecommunications Conference - GLOBECOM 2011, pp. 1-5, 2011.
[36] I. Abdo et al., "A Bi-Directional 300-GHz-Band Phased-Array Transceiver in 65-nm CMOS With Outphasing Transmitting Mode and LO Emission Cancellation," in IEEE Journal of Solid-State Circuits, vol. 57, no. 8, pp. 2292-2308, 2022.
[37] B. Yu et al., "A 200-GHz Four-Element Phased-Array Receiver System-in-Package Using HTCC Technology for Sub-Terahertz Communications," in IEEE Transactions on Microwave Theory and Techniques, vol. 72, no. 7, pp. 3920-3934, 2024.
[38] J. Hebeler et al., "Wideband BPSK Transmitter Phased Array Operating at 246 GHz With ±30° Steering Range," in IEEE Access, vol. 12, pp. 51130-51137, 2024.

Bibliographies

Joel Dittmer was born in Karlsruhe, Germany, in 1995. He received the B.Sc. and M.Sc. degrees in electrical engineering from the Karlsruhe Institute of Technology, Karlsruhe, Germany, in 2020 and 2022, respectively. He joined the Institute of Photonics and Quantum Electronics (IPQ) at the Karlsruhe Institute of Technology in 2023, where he started as a research assistant in the field of optoelectronic and electronic generated Terahertz signals for wireless communications. His research interests include THz system design, THz package design, and high data rate digital signal processing.

Akanksha Bhutani earned her M.Sc. and Ph.D. in Electrical Engineering and Information Technology from the Karlsruhe Institute of Technology (KIT), Germany, in 2012 and 2019, respectively. Since 2019, she has been leading the Antennas and Packaging research group at KIT's Institute of Radio Frequency Engineering and Electronics. Her work focuses on THz antennas and packaging for radar and wireless communication. Bhutani's accolades include the "Carl Freundenberg Prize" and the "Südwestmetall Advancement Award" for her dissertation in 2019 and 2020, the IEEE Microwave Magazine Best Paper Award in 2017, and the European Microwave Week (EuMW) Best Paper Awards in 2019 and 2022 and the International IHP "Wolfgang Mehr" Fellowship Award by the Leibniz-Institut für innovative Mikroelektronik (IHP) in 2023. In 2023, she served as the Operations Officer of EuMW 2023 held in Berlin. She has authored and co-authored over 50 research papers.

Felix Beuthan is currently pursuing his bachelor's degree in electrical engineering at the Institute of Photonics and Quantum Electronics at the Karlsruhe Institute of Technology. He is currently working on his bachelor thesis with a focus on terahertz communication technologies. His research interests include optical communication systems, terahertz technologies and their applications in advanced communication networks.

Luca Valenziano received the master's degree in electrical engineering from the University of Applied Sciences Karlsruhe (HKA), Karlsruhe, Germany, in 2022. He is currently working as a Research Associate with the Institute of Radio Frequency Engineering and Electronics (IHE), Karlsruher Institute of Technology (KIT). His main fields of research interests focus on concepts for millimeter-wave (mmW) packaging and ultra-broadband packaging of electro-optical systems.

Sandrine Wagner received a B.Sc. in Electronics and Informatics from the University of Mulhouse, France in 1989. She joined Micronas GmbH in Freiburg, Germany in 1989 where she was responsible for layout and physical verification of large scale integrated semi-conductor devices. In 2010 she joined the Fraunhofer Institute for Applied Solid State Physics (IAF), Freiburg, Germany. Her main interest is the measurement of high frequency non-linear circuits.

Axel Tessmann received the Dipl.-Ing. degree in electrical engineering from the University of Karlsruhe, Germany, in 1997 and the Ph.D. degree in electrical engineering from the University of Karlsruhe, Germany, in 2006. In 1997, he joined the Microelectronics Department, Fraunhofer Institute for Applied Solid State Physics (IAF), Freiburg, Germany, where he is involved in the development of monolithically integrated circuits and subsystems for high-resolution imaging systems and high data rate wireless communication links. His main research areas are the design and packaging of millimeter-wave and submillimeter wave ICs as well as circuit simulation and linear and nonlinear device modeling. He is currently Group Manager of the millimeter wave packaging and subsystem group at the Fraunhofer IAF.

Christian Koos received the Ph.D. (Dr.-Ing.) degree in electrical engineering from the University of Karlsruhe, Karlsruhe, Germany, in 2007. He is currently a full Professor with the Karlsruhe Institute of Technology, Karlsruhe, Germany, where he is heading the Institute of Photonics and Quantum Electronics. He has co-founded several start-up companies, such as Vanguard Photonics GmbH, Vanguard Automation GmbH, SilOriX GmbH, and DeepLight SA. From 2008 to 2010, he was affiliated with the Corporate Research and Technology Department of Carl Zeiss AG in Oberkochen, Germany, where he led the technology forecast in the area of nanotechnology. He is the author of more than 140 journal papers and more than 30 patent families. His research interests include silicon photonics and hybrid integration concepts along with the associated applications in high-speed communications, optical sensing and metrology, and ultra-fast photonic-electronic signal processing. He was the recipient of several research awards and prestigious grants, such as the ERC Starting Grant in 2011 and ERC Consolidator Grant in 2017.

Thomas Zwick (Fellow, IEEE) received the Dipl.-Ing. (M.S.E.E.) and the Dr.-Ing. (Ph.D.E.E.) degrees from the University Karlsruhe (TH), Germany, in 1994 and 1999, respectively. From 1994 to 2001 he was a research assistant at the Institut für Hochstfrequenztechnik und Elektronik (IHE) at the University Karlsruhe (TH), Germany. In February 2001 he joined IBM as research staff member at the IBM T. J. Watson Research Center, Yorktown Heights, NY, USA. From October 2004 to September 2007, Thomas Zwick was with Siemens AG, Lindau, Germany. During this period he managed the RF development team for automotive radars. In October 2007, he became a full professor at the Karlsruhe Institute of Technology (KIT), Germany. He is the director of the Institut für Hochfrequenztechnik und Elektronik (IHE) at the KIT.

Sebastian Randel (Senior Member, IEEE) received the Dr.-Ing. degree for his work on high-speed optical-time-division-multiplexed transmission systems from Technische Universität Berlin, Berlin, Germany, in 2005. He is currently a full Professor with the Karlsruhe Institute of Technology, Karlsruhe, Germany, where he is co-heading the Institute of Photonics and Quantum Electronics. From 2005 to 2010, he was a Research Scientist with Siemens Corporate Technology, Munich, Germany, where he led research and standardization activities in the fields of polymer-optical-fiber communications, visible-light communications, and optical access networks. From 2010 to 2016, he was a Member of Technical Staff with Bell Laboratories, Holmdel, NJ, USA. His current research focuses on high-capacity power-efficient optical and sub-THz communication systems and networks.